Obstacle-insensitive eigenfields due to boundary condition–symmetry compatibility

Yi-Xin Xiao and C. T. Chan*

Department of Physics, Hong Kong University of Science and Technology, Hong Kong, China

(Received 31 July 2024; accepted 13 August 2024; published 30 August 2024)

It is known that the eigenspectra and eigenfields of wave systems are sensitive to boundary conditions. We show a counterintuitive result that two hard-boundary sound cavities of different boundary shapes and of different sizes have a common set of eigenfrequencies. Moreover, their eigenfields at shared frequencies are the same in some of their common subregions. The reason is that both cavities can be created by cutting along locally mirror-symmetric lines in a honeycomb lattice, with their boundaries compatible with the hexagonal cavity's eigenfields at those common eigenfrequencies. Based on this observation, we have discovered a phenomenon where cavity eigenfields remain unaffected by obstacles of certain shapes within the cavity. The key lies in aligning the obstacles' boundaries with the antinodal lines of the cavity eigenfields, which are easy to find when the cavity contains some local mirror symmetries. All the results can be generalized to electromagnetic waves and three-dimensional cavities.

DOI: 10.1103/PhysRevB.110.075435

I. INTRODUCTION

After decades of searching, a hat-shaped monotile that can only form aperiodic tilings has been discovered [1]. This monotile has been extended to a continuous family of shapes, including a turtle-shaped monotile, by adjusting two parameters that define the shape [2]. The discovery has ignited curiosity beyond the realm of mathematics. It was not long before physicists found interesting graphenelike properties in a lattice system comprising hat tiles [3]. The discovery of monotile also inspired the discovery of quasicrystalline tilings with C_6 symmetry [4] and monotiling-based dimer model with exact solutions [5].

Inspired by the fascinating aperiodic monotile, we wonder whether a two-dimensional (2D) sound cavity with the shape of a monotile, hat or turtle, exhibits unique characteristics in its eigenfield. We hypothesize that a hat- or turtle-shaped cavity, along with its specific eigenfield, can tile the plane in such a way that the eigenfields in adjacent cavities connect smoothly. Our study reveals that some eigenmodes indeed align with the hypothesis and they display regular patterns. Moreover, a larger pattern tiled by one of these eigenmodes exhibits C_{6v} symmetry locally around some points, which implies a connection between the hat- (turtle)-shaped cavity and a regular hexagonal cavity. Further studies reveal that these three cavities share an infinite number of common eigenfrequencies, corresponding to the regular eigenmodes previously mentioned in the hat- and turtle-shaped cavities. The phenomenon of common eigenfrequencies between different cavities can be well explained from the perspective of symmetries. Building upon the above results of common eigenfrequencies, we introduce an idea that eigenfields within a cavity can exhibit insensitivity to embedded obstacles of specific shapes. All the results can also be extended to electromagnetic (EM) cavities and three dimensions.

II. COMMON EIGENFREQUENCIES FOR HAT-SHAPED AND TURTLE-SHAPED CAVITIES

The hat-shaped and turtle-shaped monotiles that can only form aperiodic tilings are shown in Figs. 1(a) and 1(b), respectively. The size and shape of the monotile are uniquely determined by two length parameters, a and b, while the angles are fixed to be one of $\{\frac{\pi}{2}, \frac{3\pi}{2}, \frac{2\pi}{3}, \frac{4\pi}{3}\}$, as shown in Fig. 1. We have $b = \sqrt{3}a$ for the hat shape and $b = \sqrt{3}a/3$ for the turtle shape. Varying the ratio a/b leads to a continuous family of monotiles [2]. In this work, 2D sound cavities in the shape of a hat and a turtle are considered. Without loss of generality, we take $b = \sqrt{3}a = \frac{\sqrt{3}}{2}m$ and $b = \frac{\sqrt{3}a}{3} = \frac{1}{2}m$ for the hat-shaped and turtle-shaped cavities, respectively.

The eigenvalue problem for a sound cavity, also known as the Laplacian eigenvalue problem, is described by the Helmholtz equation $(\nabla^2 + k^2)p = 0$, where p represents the pressure field and $k = \omega/c$ denotes the wave number, with ω and c being the angular frequency and sound velocity in air. We consider sound cavities with hard boundaries, i.e., Neumann boundary condition $\partial_n p = 0$, where ∂_n denotes the normal derivative at the boundaries. We compute the eigenfrequencies and eigenfields using the finite-element method.

Let us start with the hat-shaped cavity. Due to its irregular shape and lack of apparent symmetry, we do not expect a high degree of regularity in the cavity eigenmodes. Some of the eigenmodes indeed have rather irregular patterns as illustrated in Fig. 2(a). However, there are also many cavity modes that exhibit highly regular field patterns, of which the two lowest ones at 229 and 396 Hz are shown in Fig. 2(b). Figure 2(c) shows that a tiling of hat-shaped structures with the field pattern at 229 Hz forms a larger structure. The simple tiling of

*Contact author: phchan@ust.hk

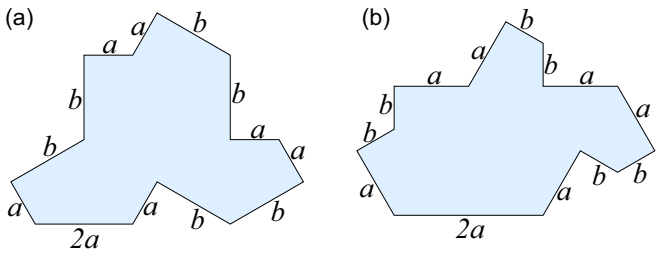

FIG. 1. The monotiles in the shape of (a) a hat and (b) an upside-down turtle. The length parameters are assumed to be $b = \sqrt{3}a$ in (a) and $b = \sqrt{3}a/3$ in (b), respectively.

the field becomes the eigenmode of the larger structure, which aligns with our hypothesis that the fields in any two neighboring cavities connect smoothly. The field pattern shown in Fig. 2(c) displays C_{6v} symmetry locally around several points and appears as if the eigenfields of regular hexagonal cavities were pieced together. Similar results are also found for the turtle-shaped cavity. These results prompt us to investigate the connection between the hat- (turtle)-shaped cavity and the regular hexagonal cavity in terms of their eigenspectra and eigenfields.

We computed the eigenfields of 2D acoustic cavities in the shape of the hat, turtle, regular hexagon, and 30 °–60 °–90 ° triangle, noting that the latter is the basic building block of the other three shapes [see Figs. 3(b)–3(e)]. Figure 3(a) depicts their eigenspectra as blue, orange, green, and red lines, respectively. We found that the spectra of the hat, turtle, and regular hexagon share a common subset that coincides with the spectrum of the triangle, which is labeled accordingly. The eigenfields of the four cavities in different shapes at the two lowest common frequencies, 229 and 396 Hz, are depicted in the first and second rows of Figs. 3(b)–3(e). Some auxiliary lines in Figs. 3(b)–3(d) are used to divide the shapes into 30 °−60 °−90 ° triangles, each of which has the same field pattern as those displayed in Fig. 3(e).

We will provide a detailed account for the phenomenon of common eigenfrequencies shown in Fig. 3 from the aspect of symmetry in Sec. III.

III. EXPLANATION FROM A SYMMETRY PERSPECTIVE

The point group for a regular hexagonal cavity can be denoted by $C_{6v} = \{E, C_2, 2C_3, 2C_6, 3\sigma_x, 3\sigma_y\}$, which includes

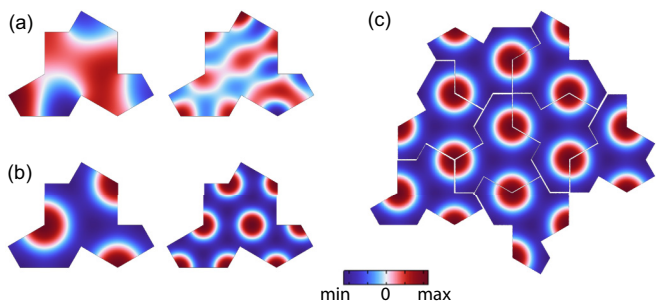

FIG. 2. (a) Examples of irregular eigenfields of a hat-shaped acoustic cavity. (b) Examples of regular fields. (c) A tiling of regular eigenfields of the hat-shaped cavity exhibits locally C_{6v}-symmetric pattern.

the identity, inversion, two rotations of $\pm\frac{2\pi}{3}$, two rotations of $\pm\frac{\pi}{3}$, and six reflections pertaining to two different types of mirror axes.

The cavity eigenfields can be classified into eight classes based on their even or odd parity under mirror-symmetry operations, as shown in Fig. 4 [6,7]. The eigenfields in each class are even (odd) with respect to the solid (dashed) lines. Each class is labeled by a notation like "++a" and illustrated by an eigenmode. The first "±" in the notation means even (odd) parity with respect to $x \to -x$, and the second "±" represents even (odd) parity with respect to $y \to -y$. The letters "a" and "b" distinguish between eigenmodes that involve two and six mirror-symmetry lines, respectively. There are six irreducible representations (irreps) for C_{6v}: four one-dimensional irreps (A_1, A_2, B_1, and B_2) and two 2D irreps (E_1 and E_2), as labeled in Fig. 4 next to each eigenfield class [8,9].

For eigenfields in the six classes shown in columns 2–4 of Fig. 4, nodal lines with $p = 0$ appear at the dashed lines. The eigenfield and eigenvalue will remain unchanged if we place a soft boundary at a nodal line, since the soft boundary condition $p = 0$ is satisfied there. Similarly, for the six classes shown in columns 1, 3, and 4 of Fig. 4, the eigenfields will have antinodal lines at the solid lines, where the normal derivative of pressure vanishes, i.e.,$\partial_n p = 0$. If we place hard boundaries at these antinodal lines, the eigenfield and eigenvalue do not change since the hard boundary condition $\partial_n p = 0$ is already satisfied there. We refer to such a cooperation between the hard boundary conditions and mirror symmetries as boundary condition–symmetry compatibility. It explains why the triangle and hexagon share some eigenfrequencies and dictates how their eigenfields are related at the shared frequencies as illustrated in Fig. 3.

We now use the 30 °−60 °−90 ° triangles with hard-wall boundaries together with their eigenfields as building blocks. By tiling the space with this triangular building block, we can create the the hat and turtle structures. By removing the interior hard boundaries of the triangles, the eigenfields will automatically become the eigenmodes of the bigger hat (turtle) at the same frequency [see Figs. 3(b) and 3(c)] because the boundary conditions are satisfied. The eigenfields are obviously symmetric between each pair of adjacent triangles in the building process. In this way, the boundary condition–symmetry compatibility is used. Similarly, we can use the triangular building blocks to tile the eigenfields of the regular hexagon that fall under the $++b$ class shown in Fig. 4. Since the eigenfields of the 30 °−60 °−90 ° triangle serve as the basic unit for tiling some eigenfields of the hat, turtle, and regular hexagon, the spectrum of the triangle must be a common subset of the spectra for the latter three shapes. It is now easy to comprehend why the regular eigenfield of the hat (turtle), when tiled together, exhibits local C_{6v} symmetry around some points. The fact that the hat (turtle) shares the same tiling unit as the highly symmetric regular hexagon can be viewed as a latent symmetry in the hat (turtle), where the high regularity of some eigenmodes is not a direct consequence of the symmetry of the overall structure but originates from more subtle mechanisms.

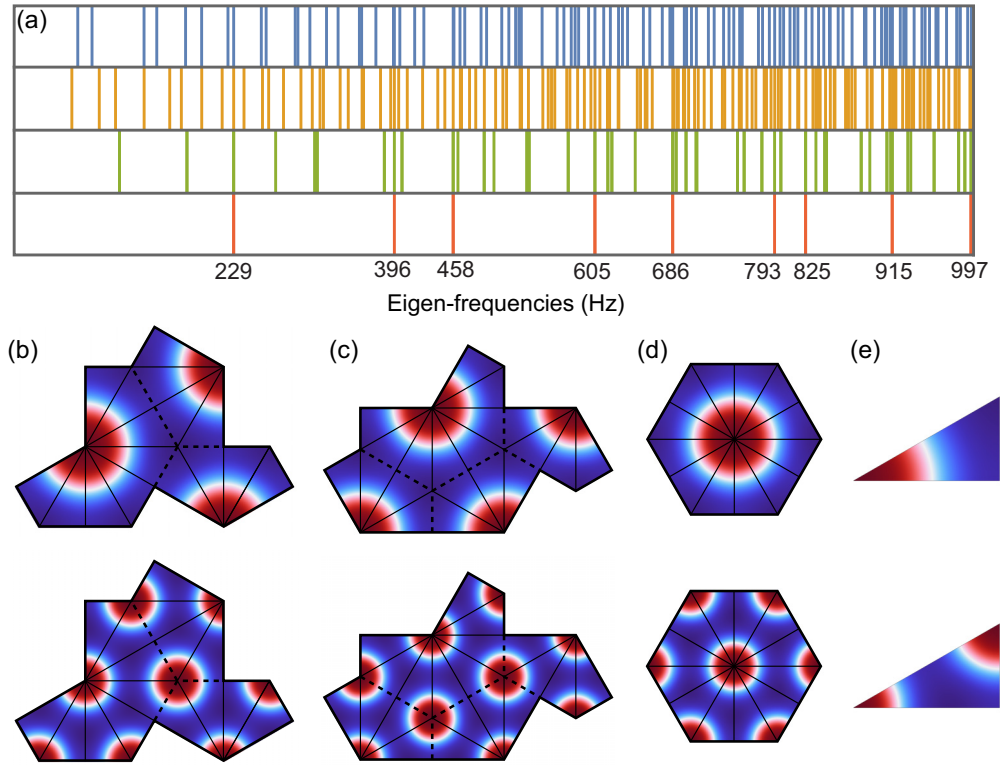

FIG. 3. (a) Spectral overlap among the hard-boundary cavities in the shape of a hat (blue), a turtle (orange), a regular hexagon (green), and a $30°-60°-90°$ triangle (red). (b)–(e) The eigenmodes of the hat, the turtle (inverted), the regular hexagon, and the triangle at their common frequencies: 229 Hz (first row) and 396 Hz (second row).

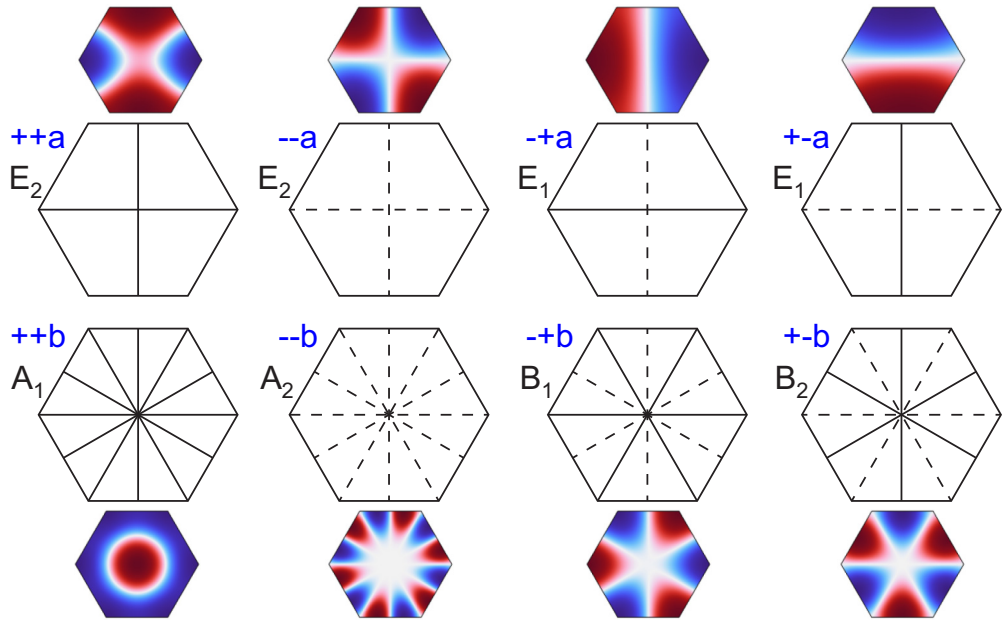

FIG. 4. The eight classes of the eigenfields of the hexagonal cavity. The eigenfields are even (odd) about the solid (dashed) lines. In the notation "+−a", "+−" means that the wave function is even with respect to $x \to -x$ and odd with respect to $y \to -y$. The notations "a" and "b" represent the involvement of two and six mirror-symmetry lines, respectively. The labels A_1, A_2, B_1, B_2 and E_1, E_2 denote the corresponding one-dimensional and two-dimensional irreducible representations, respectively.

The common eigenfrequencies, i.e., the spectrum of the $30°-60°-90°$ triangle in Fig. 3(e), are given by

$$f_c = \frac{2c}{3L}\sqrt{m^2+mn+n^2}, \tag{1}$$

where $n \geqslant m \geqslant 0$ and $m, n \in \mathbb{Z}$, and $c = 343$ m/s and $L = 1$ m are the acoustic speed in air and the length of the hypotenuse of the $30°-60°-90°$ triangle, respectively [10,11]. Here, we used the fact that the $30°-60°-90°$ triangular cavity with hard boundaries has the same spectrum as the equilateral triangular cavity, except that it does not exhibit degeneracies. The reason is that there is an even mode at every eigenfrequency for the equilateral triangular cavity, possibly besides a degenerate odd partner, and each even mode corresponds to a mode of the $30°-60°-90°$ triangular cavity.

Weyl's law tells us the number of eigenvalues of the Laplace operator smaller than λ is given by $N(\lambda) \propto \frac{\omega_d \mu_d}{(2\pi)^d}\lambda^{d/2}$ for $\lambda \to \infty$, where d denotes the dimension of the system, μ_d is the area (volume) for $d = 2$ ($d = 3$), and $\omega_d = \frac{\pi^{d/2}}{\Gamma(d/2+1)}$ is the volume of the unit ball in d dimensions [12]. Therefore, using Weyl's law, the ratio of common frequencies to the entire spectrum of the hat-shaped cavity is estimated to be

$$r_{\text{hat}} = \frac{S_\Delta}{S_{\text{hat}}} = \frac{1}{16}, \tag{2}$$

where S_Δ and S_{hat} denote the areas of the $30°-60°-90°$ triangle and the hat shape in Figs. 3(b) and 3(e), respectively. That is, modes that exhibit regular patterns pertaining to the $++b$ hexagonal modes account for about $1/16$ of all modes of the hat-shaped cavity. Similarly, we have $r_{\text{turtle}} = S_\Delta/S_{\text{turtle}} = 1/20$ for the turtle-shaped cavity.

An alternative perspective is that the eigenfields of the hat (turtle), for the common frequencies, can be viewed as cutouts from the eigenfields of hexagons that are pieced together. This is suggested by the auxiliary lines in Figs. 3(b) and 3(c). To ensure that the hard boundary condition $\partial_n p = 0$ is met at the boundaries of the hat (turtle), it is necessary for the cutting path to align with the antinodal lines of the fields. This alignment renders boundary condition–symmetry compatibility. This requirement selects all the eigenmodes of a hexagon that belong to the $++b$ class illustrated in Fig. 4. The perspective of cutting also clarifies why the hat, turtle, and hexagon share a common set of eigenfrequencies that correspond to the $30°-60°-90°$ triangle.

We point out that an arbitrarily shaped cavity can exhibit antinodal lines in its eigenfields. By cutting along the antinodal lines of a specific eigenfield at an eigenfrequency, say f_0, we create a smaller cavity. Under hard boundary conditions, this smaller cavity will also have the same eigenfrequency f_0. However, without symmetries involved, the two cavities generally will not share other common frequencies. Moreover, the cutting path cannot be determined until an eigenfield is computed to give us the antinodal lines, which contrasts with our cavities pertaining to regular hexagons.

It is worth noting that both the construction and cutting approaches need only to consider the boundary conditions related to the gluing or cutting operation, as the Helmholtz equation is satisfied elsewhere. We found that some eigenmodes belonging to the $++b$ class have a degenerate partner in the $-+b$ class. However, these $-+b$ modes are eliminated by the cutting procedure as the hard boundary condition is not satisfied along the whole cutting path. Besides the hat (turtle) shapes, these methods can be used to create other shapes that share some eigenfrequencies with a regular hexagon and may not be able to tile the plane. One can also substitute another symmetric shape for the regular hexagon.

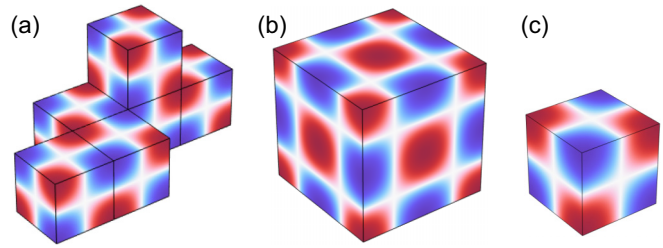

FIG. 5. (a)–(c) The eigenmodes at a common frequency of 594 Hz for the 3D sound cavities with hard boundaries. The cavities in (a) and (b) can be constructed by using 6 and 8 smaller cubic cavities in (c), respectively. The cube in (c) has a side length of 0.5 m.

It should be emphasized that the occurrence of shared eigenfrequencies among 2D cavities of different shapes can be extended to three dimensions by assigning those 2D cavities with heights of $Z_1 h, Z_1 h, Z_3 h$, and so on, where h is any height and Z_i are integers. We can also achieve the goal by constructing distinct three-dimensional (3D) cavities by using the same 3D basic block, where boundary condition–symmetry compatibility is implicitly utilized. For illustration, Fig. 5 displays the eigenmodes of 3D cavities at their common eigenfrequency of 594 Hz. The smaller cubic cavity in Fig. 5(c) is the basic block to build the cavities in Figs. 5(a) and 5(b). There are infinitely many other common eigenfrequencies for the three cavities, which constitute the spectrum of the cavity in Fig. 5(c).

Furthermore, the phenomenon of shared eigenfrequencies can be generalized to 2D EM cavities with perfect electric conductor (PEC) boundaries and air/dielectric filling, noting that the H_z field in a 2D PEC cavity acts like the pressure field p in a 2D acoustic cavity. For a 3D PEC cavity that is uniform in z and has a height of h, the H_z field for the TE cavity modes also satisfies the Helmholtz equation like sound waves in 2D cavities, apart from a simple dependence on z, that is, $\sin(\frac{p\pi z}{h})$, $p = 1, 2\cdots$. Therefore, we can achieve shared eigenfrequencies among TE modes in different 2D/3D PEC cavities as we have done for sound cavities. The story for the E_z field of TM cavity mode is slightly different: (1) It is Dirichlet boundary condition at the PEC side walls that needs to be satisfied by E_z, which corresponds to soft boundary condition for sound waves; and (2) The dependence on z becomes $\cos(\frac{p\pi z}{h})$, $p = 0, 1, 2\cdots$. With (1), the boundary condition–symmetry compatibility required to achieve shared eigenfrequencies among TM modes in different PEC cavities changes accordingly, that is, the fields in every neighboring pair of basic building blocks need to exhibit odd parity instead of even parity.

IV. CAVITY EIGENFIELDS INSENSITIVE TO OBSTACLES

In a typical situation, when an object is inserted into a cavity, we expect the cavity's eigenmode frequency to change.

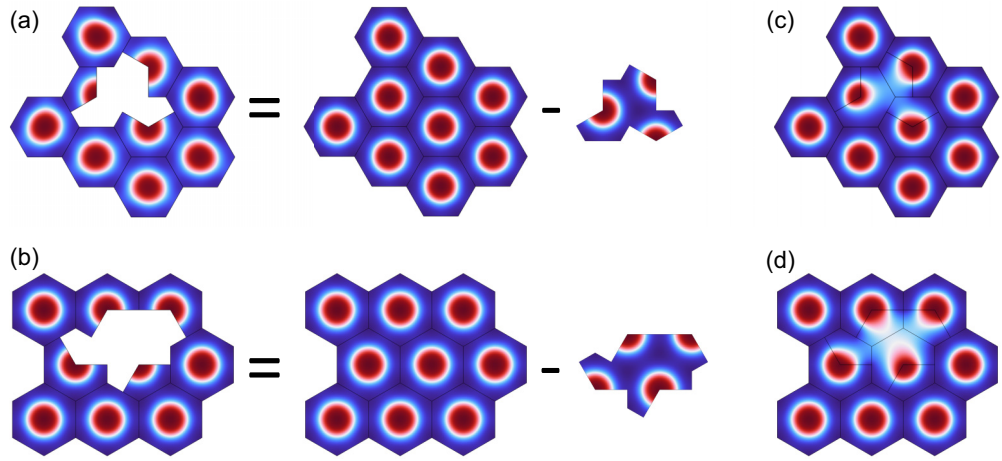

FIG. 6. Insensitivity of 2D acoustic cavity eigenfields to (a) a hat-shaped or (b) a turtle-shaped obstacle with hard boundaries. (c), (d) Replacing the hard obstacle with a steel hat-shaped or turtle-shaped obstacle has negligible effect on the cavity eigenfields outside the obstacle.

Inspired by the observation of shared eigenfrequencies among cavities of different sizes and shapes, we have found a remarkable event where the eigenfields of a cavity remain unaltered by obstacles of specific shapes inserted into the cavity. Figures 6(a) and 6(b) demonstrate that the eigenfields as well as the eigenfrequencies remain unchanged when a hat- (turtle)-shaped hard obstacle is inserted into the cavity. This occurs because of boundary condition–symmetry compatibility: The cutting path, which creates hard boundaries, aligns with the antinodal lines of the eigenfield (i.e., the local mirror-symmetry lines) in the large cavity. The insensitivity to obstacles applies to infinitely many eigenfields that correspond to the ++b class in Fig. 4. This occurrence can be extended to cavities and obstacles in different shapes.

While hard-wall boundary conditions are idealized constructs, in practical situations, steel and other rigid materials can serve as hard walls when they create an interface with an air domain, due to the significant impedance mismatch between them. We can opt to replace the perfectly hard walls in Figs. 6(a) and 6(b) with hat- (turtle)-shaped steel obstacles, as depicted in Figs. 6(c) and 6(d). As expected, the eigenfields relevant to the ++b class exhibit negligible changes in the presence of obstacles, and their eigenfrequencies remain largely unaltered. We can approximate the steel region surrounded by air as a cavity with soft boundaries. This cavity has its lowest eigenmode at 2269 Hz. As the frequency increases, the steel obstacle gradually stops acting like a hard wall, allowing pressure fields inside it. Consequently, the insensitivity deteriorates and eventually vanishes at higher frequencies. The simulations indicate that the insensitivity observed at 229 Hz in Fig. 6(c) holds almost perfectly up to around 1600 Hz.

The insensitivity of eigenfields to obstacles inside a cavity occurs more frequently than initially expected. For illustration, the eigenfield insensitivity can also be observed in a square-shaped cavity that contains an obstacle in the shape of the so-called isospectral pair of geometries depicted in Figs. 7(a) and 7(b) [13,14]. Isospectrality refers to the property that two nonisometric cavities have identical eigenvalue spectrum [13,14]. The isospectrality between the cavities depicted in Figs. 7(a) and 7(b) is shown by the overlapping blue and orange lines in Fig. 7(e). The isospectral pair as well as the square in Fig. 7(c) can be built using the isosceles right triangle in Fig. 7(d) as the building block. Consequently, the isospectral pair and the square share a set of eigenfrequencies that make up the spectrum of the isosceles right triangle. This is demonstrated in Fig. 7(e), where the blue, orange, green, and red lines correspond to the spectra of the cavities listed in Figs. 7(a)–7(d), respectively. Figures 7(a)–7(d) display the eigenfields of the four cavities at their second-lowest common frequency, $f = 243$ Hz. When a hard obstacle in the shape of either of the isospectral pair is placed inside the square cavity, the eigenfield for any common eigenfrequency remains unaffected outside the obstacle. This is depicted in Fig. 7(c), where the obstacle is represented by the magenta/green dashed lines.

The eigenfield insensitivity to obstacles can be extended to three dimensions and EM cavities as per our discussions at the end of Sec. III.

V. CONCLUSIONS AND DISCUSSION

We have shown a rather counterintuitive result that a hat-shaped sound cavity and a turtle-shaped sound cavity, despite their different boundary shapes and sizes, have a set of eigenfrequencies in common. By tiling the eigenfields of a hat-shaped (or turtle-shaped) cavity at those common frequencies, we can obtain a pattern that locally resembles the eigenfields of a regular hexagonal cavity in the ++b class. We explained this by boundary condition–symmetry compatibility. Specifically, all the hard boundaries of the hat (turtle) can be aligned with the antinodal lines, due to mirror symmetries, of the ++b eigenfields of the regular hexagon. As a result, some eigenfields of the hat (turtle) cavity can be obtained by placing a hard-boundary hat (turtle) at the antinodal lines of the ++b eigenfields of several hexagons tiled together, without changing the eigenfrequencies. Furthermore, based on the observation of shared eigenfrequencies among distinct cavities, we have discovered an unexpected phenomenon where cavity eigenfields remain unaffected by obstacles of certain shapes within the cavity. We emphasize that the findings can be extended to EM waves and three dimensions.

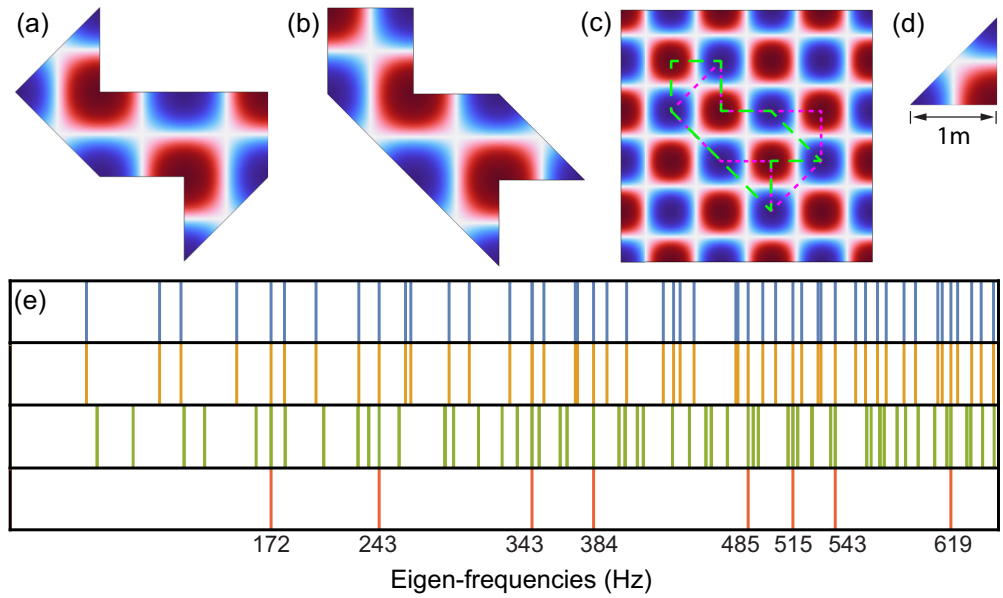

FIG. 7. (a)–(d) Eigenfields of four sound cavities at 243 Hz, including (a), (b) an isospectral pair, (c) a square, and (d) an isosceles right triangle. (c) also shows that inserting a hard obstacle in the shape of (a) or (b) inside the square does not alter the eigenfield. (e) The spectra of the four cavities in (a)–(d) are represented by the blue, orange, green, and red lines, respectively. They share common frequencies that form the spectrum of the isosceles right triangle.

The existence of a set of common eigenfrequencies shared among cavities with different geometries reminds us of isospectral billiards, which refer to nonisometric billiards with identical eigenvalue spectrum [13,14]. The discovery of 2D isospectral billiards answered Kac's celebrated question, "Can one hear the shape of a drum?" with a definitive "no" [13–16]. Kac's question, along with isospectral billiards, has greatly stimulated research on a range of inverse spectral problems [16–24]. Our research demonstrates that different cavities can be partially isospectral: While not all their modes have the same frequencies, they do share a certain percentage of resonant frequencies. The partially isospectral cavities we discovered can be seen as an extended and less strict version of isospectral billiards, which improves our understanding of how the cavity's shape relates to its eigenfrequencies. Constructing partially isospectral billiards (or cavities) is straightforward when applying the concept of boundary condition–symmetry compatibility, which requires each pair of adjacent basic building blocks to be symmetrically arranged. It contrasts sharply with the formidable challenge of finding fully isospectral billiards.

Our work on insensitivity of cavity eigenfields to obstacles bears resemblance to invisibility cloaking and related inverse problems [19,20,25–31] since we cannot detect the presence of obstacles solely through observation of cavity eigenfields. Moreover, the imperceptibility of the obstacles holds true at a series of frequencies, unlike most invisibility cloaks that function at only a single frequency.

ACKNOWLEDGMENTS

We thank Z.-Q. Zhang and K. H. Fung for their helpful discussions and suggestions. This work is supported by Research Grants Council (RGC) Hong Kong (Grant No. AoE/P-502/20).

[1] D. Smith, J. S. Myers, C. S. Kaplan, and C. Goodman-Strauss, An aperiodic monotile, Comb. Theory **4**, 6 (2024).
[2] D. Smith, J. S. Myers, C. S. Kaplan, and C. Goodman-Strauss, A chiral aperiodic monotile, arXiv:2305.17743.
[3] J. Schirmann, S. Franca, F. Flicker, and A. G. Grushin, Physical properties of an aperiodic monotile with graphene-like features, chirality, and zero modes, Phys. Rev. Lett. **132**, 086402 (2024).
[4] J. E. S. Socolar, Quasicrystalline structure of the hat monotile tilings, Phys. Rev. B **108**, 224109 (2023).
[5] S. Singh and F. Flicker, Exact solution to the quantum and classical dimer models on the spectre aperiodic monotiling, Phys. Rev. B **109**, L220303 (2024).
[6] Jan Wiersig, Hexagonal dielectric resonators and microcrystal lasers, Phys. Rev. A **67**, 023807 (2003).
[7] L. M. Cureton and J. R. Kuttler, Eigenvalues of the Laplacian on regular polygons and polygons resulting from their disection, J. Sound Vibr. **220**, 83 (1999).
[8] T. Inui, Y. Tanabe, and Y. Onodera, *Group Theory and its Application in Physic* (Springer, Berlin, 1996).
[9] K. Sakoda, *Optical Properties of Photonic Crystals* (Springer, New York, 2005).
[10] B. J. McCartin, *Laplacian Eigenstructure of the Equilateral Triangle* (Hikari, Rousse, 2011).
[11] D. S. Grebenkov and B.-T. Nguyen, Geometrical structure of Laplacian eigenfunctions, SIAM Rev. **55**, 601 (2013).

[12] V. Ivrii, 100 years of Weyl's law, Bull. Math. Sci. **6**, 379 (2016).
[13] C. Gordon, D. Webb, and S. Wolpert, Isospectral plane domains and surfaces via Riemannian orbifolds, Invent. Math. **110**, 1 (1992).
[14] C. Gordon, D. L. Webb, and S. Wolpert, One cannot hear the shape of a drum, Bull. Amer. Math. Soc. **27**, 134 (1992).
[15] M. Kac, Can one hear the shape of a drum, Am. Math. Mon. **73**, 1 (1966).
[16] O. Giraud and K. Thas, Hearing shapes of drums: Mathematical and physical aspects of isospectrality, Rev. Mod. Phys. **82**, 2213 (2010).
[17] K. Chadan, D. Colton, L. Päivärinta, and W. Rundell, *An Introduction to Inverse Scattering and Inverse Spectral Problems* (SIAM, Philadelphia, 1997).
[18] J. Pöschel and E. Trubowitz, *Inverse Spectral Theory* (Academic Press, New York, 1987).
[19] A. Greenleaf, M. Lassas, and G. Uhlmann, On nonuniqueness for Calderón's inverse problem, Math. Res. Lett. **10**, 685 (2003).
[20] A. Greenleaf, M. Lassas, and G. Uhlmann, Anisotropic conductivities that cannot be detected by EIT, Physiol. Meas. **24**, 413 (2003).
[21] O. Hul, M. Ławniczak, S. Bauch, A. Sawicki, M. Kuś, and L. Sirko, Are scattering properties of graphs uniquely connected to their shapes? Phys. Rev. Lett. **109**, 040402 (2012).
[22] N. Shemesh, C.-F. Westin, and Y. Cohen, Magnetic resonance imaging by synergistic diffusion-diffraction patterns, Phys. Rev. Lett. **108**, 058103 (2012).
[23] S. V. Lenz, S. Guenneau, B. W. Drinkwater, R. V. Craster, and M. W. Holderied, Transformation twinning to create isospectral cavities, Phys. Rev. B **108**, 064209 (2023).
[24] Y. Zhao and M. M. Fogler, Shape prediction on the basis of spectrum using neural networks, Phys. Rev. Res. **5**, 013110 (2023).
[25] J. B. Pendry, D. Schurig, and D. R. Smith, Controlling electromagnetic fields, Science **312**, 1780 (2006).
[26] U. Leonhardt, Optical conformal mapping, Science **312**, 1777 (2006).
[27] D. Schurig, J. J. Mock, B. J. Justice, S. A. Cummer, J. B. Pendry, A. F. Starr, and D. R. Smith, Metamaterial electromagnetic cloak at microwave frequencies, Science **314**, 977 (2006).
[28] J. Li and J. B. Pendry, Hiding under the carpet: A new strategy for cloaking, Phys. Rev. Lett. **101**, 203901 (2008).
[29] Y. Lai, H. Chen, Z.-Q. Zhang, and C. T. Chan, Complementary media invisibility cloak that cloaks objects at a distance outside the cloaking shell, Phys. Rev. Lett. **102**, 093901 (2009).
[30] H. Chen and C. T. Chan, Acoustic cloaking and transformation acoustics, J. Phys. D: Appl. Phys. **43**, 113001 (2010).
[31] S. Zhang, C. Xia, and N. Fang, Broadband acoustic cloak for ultrasound waves, Phys. Rev. Lett. **106**, 024301 (2011).